Contents lists available at ScienceDirect

Coastal Engineering

journal homepage: www.elsevier.com/locate/coastaleng

Climate controls on longshore sediment transport and coastal morphology adjacent to engineered inlets

Andrew W. Stevens [a,*], Peter Ruggiero [b], Kai A. Parker [a], Sean Vitousek [a], Guy Gelfenbaum [a], George M. Kaminsky [c]

[a] U.S. Geological Survey, Santa Cruz, CA, USA
[b] Oregon State University, Corvallis, OR, USA
[c] Washington State Department of Ecology, Olympia, WA, USA

ARTICLE INFO

Original content: Beach topography and nearshore bathymetry of the Columbia River littoral cell, Washington and Oregon (ver. 4.0, January 2024) (Original data)
Wave model setup and selected output (Original data)
Southwest Washington littoral drift restoration—Beach and nearshore morphological monitoring (Original data)

Keywords:
Longshore transport
Wave modeling
Climate indices
Columbia River

ABSTRACT

Coastal jetties are commonly used throughout the world to stabilize channels and improve navigation through inlets. These engineered structures form artificial boundaries to littoral cells by reducing wave-driven longshore sediment transport across inlet entrances. Consequently, beaches adjacent to engineered inlets are subject to large gradients in longshore transport rates and are highly sensitive to changes in wave climate. Here, we quantify annual beach and nearshore sediment volume changes over a 9-yr time period along 80 km of wave-dominated coastlines in the U.S. Pacific Northwest. Beach and nearshore monitoring during the study period (2014–2023) reveal spatially coherent, multi-annual patterns of erosion and deposition on opposing sides of two engineered inlets, indicating a regional reversal of longshore-transport direction. A numerical wave model coupled with a longshore transport predictor was calibrated and validated to explore the causes for the observed spatial and temporal patterns of erosion and deposition adjacent to the inlets. The model results indicate that subtle but important changes in wave direction on seasonal to multi-annual time scales were responsible for the reversal in the net longshore sediment transport direction and opposing patterns of morphology change. Changes in longshore transport direction coincided with a reversal in the Pacific Decadal Oscillation (PDO) climate index, suggesting large-scale, multi-decadal climate variability may influence patterns of waves and sediment dynamics at other sites throughout the Pacific basin.

1. Introduction

Many approaches have been developed to predict coastal morphological change (Hunt et al., 2023) and quantify sediment transport pathways (Pearson et al., 2020), with much attention focused on open-ocean, wave-dominated sandy beaches. Estuarine and tidal inlets, however, are particularly dynamic and complex coastal landscapes with morphologies determined by continuous fluvial, tidal, and wave-driven exchanges of water and sediment between the inlet basin and adjacent ocean (e.g., Elias et al., 2019). Humans disrupt natural sediment transport processes at inlets through the construction of jetties and dredging of navigation channels (Kaminsky et al., 2010). Humans also alter transport processes indirectly by modifying sediment supplies with dam construction (Ritchie et al., 2018) or upstream land-use practices (Barnard et al., 2013). Effective management of inlet and adjacent coastal systems seeking to maintain the many transportation and ecosystem services they provide rely on accurate monitoring and robust predictions of sediment transport and coastal evolution at a variety of temporal and spatial scales.

A general lack of observations has limited our ability to understand and predict coastal morphological change and quantify sediment budgets (Splinter and Coco, 2021). In some coastal environments, the recent expansion of remote-sensing techniques is enhancing our understanding of coastal processes and coastal change (Vitousek et al., 2022). For example, satellite derived shorelines have enabled researchers to estimate shoreline erosion and accretion trends at global scale (Luijendijk et al., 2018), better understand connections between watershed and coastal processes (Warrick et al., 2022), quantify climate-driven shoreline variability (Vos et al., 2023), and improve numerical models through data assimilation (Vitousek et al., 2023). Widely available and accurate satellite derived observations of coastal change are, however, mostly limited to portions of the subaerial beach and therefore do not

* Corresponding author.
E-mail address: astevens@usgs.gov (A.W. Stevens).

https://doi.org/10.1016/j.coastaleng.2024.104617
Received 20 June 2024; Received in revised form 27 August 2024; Accepted 16 September 2024

include subaqueous changes. Remote sensing techniques used to quantify coastal bathymetry such as bathymetric lidar (Szafarczyk and Tos, 2022), spectral analysis of wave propagation and bathymetric inversion (Holman and Bergsma, 2021; Bergsma et al., 2021), and photogrammetry (Palaseanu-Lovejoy et al., 2023) are not currently robust, accurate, or scalable enough to support detailed quantitative change analysis over a wide range of environments or at spatial scales relevant for many coastal management issues. Long-term field datasets that document combined topographic and bathymetric change using traditional survey techniques (e.g., Ludka et al., 2019; Turner et al., 2016; Bertin et al., 2022; McCarroll et al., 2023) are therefore still relevant and sorely needed to quantify changing coastal sediment budgets and isolate the relative contributions of cross-shore and longshore processes responsible for coastal evolution (Harley et al., 2022).

Wave processes are often the primary driver of sediment transport and morphology change along sandy, ocean facing beaches (e.g., Wright and Short, 1984). Wave climates worldwide are affected by large-scale climate variability at a variety of temporal scales (Casas-Prat et al., 2024). In the Pacific Ocean basin, widespread impacts on shoreline positions have been associated with El Niño/Southern Oscillation events, including increased erosion due to elevated wave energy and water levels (Barnard et al., 2017; Vos et al., 2023) and planform rotation caused by anomalies in wave direction (Peterson et al., 1990; Ranasinghe et al., 2004). Numerical modeling performed by Anderson et al. (2018) suggested climate variability associated with the Pacific Decadal Oscillation resulted in reversals in longshore transport direction and planform rotation at multi-decadal time scales. These studies have almost entirely focused on the subaerial beach or position of the shoreline, which precludes a comprehensive understanding of the effects of wave climate variability on the full nearshore planform. Like embayed beaches (e.g., Ibaceta et al., 2023), coastal areas adjacent to inlets with jetties that interrupt longshore sediment transport are particularly sensitive to wave-direction anomalies. Thus, coastal areas adjacent to engineered inlets represent excellent case study sites to examine the effects of climate variability on coastal morphology and sediment budgets.

In this study, we present observations and analysis of coastal morphology and sand volume change based on 10 annual topographic and bathymetric surveys between 2014 and 2023 along the wave dominated shorelines of the Columbia River littoral cell, Washington and Oregon, USA. Analysis of the dataset presented here focuses on the open ocean facing beach and nearshore regions immediately adjacent to two engineered inlets that are stabilized with rock jetties and maintained with annual dredging of the navigation channels. A high-resolution numerical wave model combined with a longshore sediment transport predictor was developed to investigate the relationships between wave climate variability and changes in sediment volume along the coastal areas adjacent to the engineered inlets. The time period of our study included a very strong El Niño/Southern Oscillation event (2015–2016) and a reversal of the Pacific Decadal Oscillation index (2017–2019). We hypothesize that the coastal sediment budgets adjacent to the engineered inlets will be sensitive to large-scale climate variability and will be dominated by changes in wave direction given the jetty-constrained longshore sediment transport pathways. The detailed observations and model framework were used in combination with a simple volumetric change box model to test this hypothesis, investigate

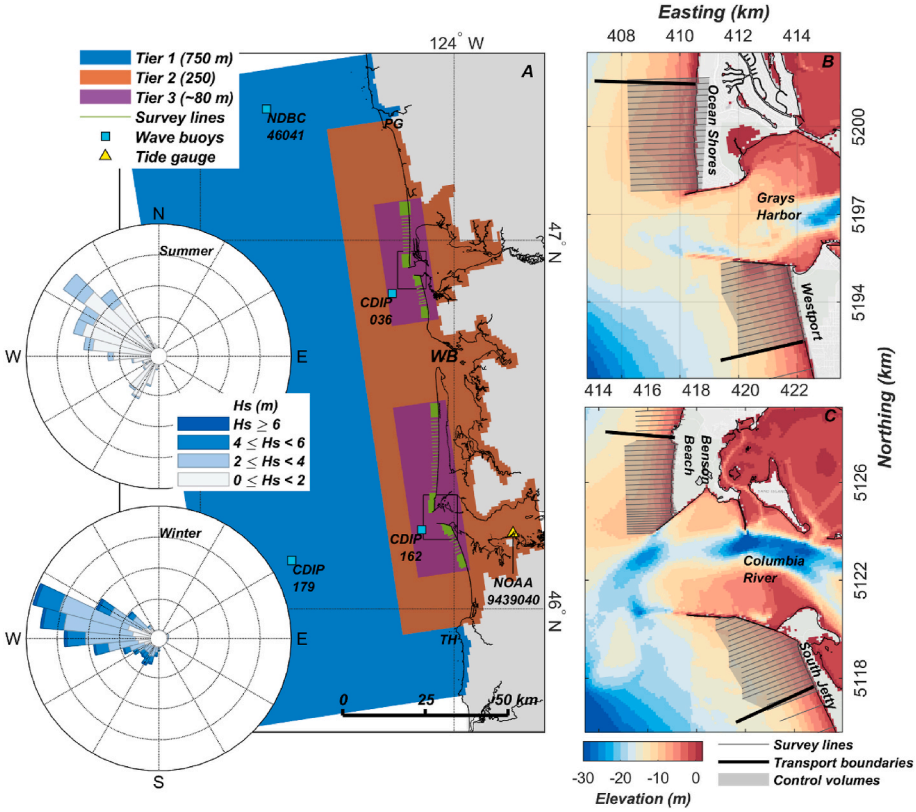


Fig. 1. Maps of study area showing, A, extents of nested wave model grids (Tiers 1–3), locations of bathymetric and topographic survey lines, wave buoys, and tide gauges. Black boxes provide the locations of the detail areas shown in B-C. B-C, Maps showing bathymetry of the engineered inlets of B, Grays Harbor, and C, the Columbia River. The locations of survey lines, control volumes where integrated sediment volume changes were computed, and boundaries used for longshore transport calculations are provided in B-C. Insets in A show distributions of wave height and direction for summer (June, July, August) and winter (December, January, February) during the study period based primarily on data obtained from CDIP buoy 179. Gaps in the wave buoy record (about 7%) were filled with model predictions for the buoy location from this study. The locations of Tillamook Head (TH), Point Grenville (PG), and Willapa Bay (WB) are denoted in A. Cartesian coordinates in panels B–C are provided in UTM Zone 10, meters.

the temporal scales and mechanisms responsible for coastal morphology change, and to inform effective sediment management strategies at engineered inlets across the region.

2. Study site

Over most of the late Holocene, the Columbia River has been the primary source of sediment to 165 km of prograding coastline between Point Grenville (PG) and Tillamook Head (TH; Fig. 1) along the northeast Pacific Ocean (Twichell et al., 2010). The Columbia River littoral cell consists of 4 barrier beach plains separated by the inlets of Grays Harbor, Willapa Bay (WB), and the Columbia River. Vegetated coastal foredunes generally back the wide, gently sloping beaches composed primarily of well sorted medium to fine sand (Ruggiero et al., 2005). Multiple dynamic subtidal and intertidal sandbars (Cohn and Ruggiero, 2016; Splinter et al., 2018; Di Leonardo and Ruggiero, 2015) typify the nearshore throughout the study area. Tides along the beaches of the Columbia River littoral cell are classified as meso-tidal, with a great diurnal range of 2.6 m (NOAA tide station 9439040).

The northeast Pacific Ocean is characterized by an extreme wave climate with a mean wave height in the winter of 3.8 m and winter storm events that routinely produce wave heights in excess of 10 m (Ruggiero et al., 2010a). The wave climate in the summer is less severe, with a mean wave height of 1.6 m. Wave energy in the winter is typically directed from the west and southwest during the passage of extratropical low-pressure systems, while high pressure systems with more modest winds and waves from the northwest are common throughout the summer (Fig. 1A). The strong seasonal variation in oceanographic forcing induces a cross-shore exchange of sediment between the beach and the nearshore, here producing relatively narrow beaches in the winter, a process that is common throughout the wave-dominated beaches of the Pacific basin (e.g., Shepard, 1950) and the Columbia River littoral cell (Antolinez et al., 2018). Longshore transport is typically directed to the north during winter storm events driven by southwest waves and to the south during the relatively calm summer conditions driven by waves from the northwest (Komar, 1998).

Large-scale climate variability modifies the typical seasonal patterns and may result in gradients in longshore transport and net volume change at interannual and longer time scales. For example, severe erosion along portions of the Columbia River littoral cell has been associated with the El Niño/Southern Oscillation (Kaminsky et al., 1998; Komar, 1998) and elsewhere throughout the Pacific Basin (Barnard et al., 2017; Vos et al., 2023). A strong El Niño event occurred during the winter of 2015 and 2016 that produced elevated water levels and increased wave energy, resulting in erosion throughout the Pacific basin, including the Columbia River littoral cell (Barnard et al., 2017). Anderson et al. (2018) suggested that multi-decadal beach rotations along the coast of Oregon were associated with changes in longshore transport directions due to the Pacific Decadal Oscillation.

Human alterations to the coastal system and upstream land-use practices have altered hydrodynamic processes, sediment fluxes, and transport pathways throughout the historical period. Rock jetties constructed at the entrances to Grays Harbor and the Columbia River between 1885 and 1939 had widespread and multi-decadal impacts resulting in shoreline progradation along much of the Columbia River littoral cell (Kaminsky et al., 2010). Changes in forestry practices and dam construction upstream resulted in a 70% reduction of sediment supplied from the Columbia River to the coast between 1935 and 1997 (Gelfenbaum and Kaminsky, 2010). Despite the reduction in sediment supply, progradation of beaches along much of the Columbia River littoral cell has continued (Ruggiero et al., 2016; Stevens et al., 2020). However, erosion hotspots persist at several locations proximal to the major inlet entrances, prompting various costly engineering interventions (e.g., Stevens et al., 2012; Allan and Gabel, 2016; Bayle et al., 2021) to protect infrastructure and reduce erosion impacts.

Annual maintenance dredging of the navigation channels at Grays Harbor and the Columbia River contribute substantially to the sediment budgets of the adjacent shorelines. Between 2 and 4 million m^3 (Mm^3) of sediment is dredged annually from the 10 km long entrance channel at Columbia River (USACE, 2023) and about 1 Mm^3 is dredged annually from Grays Harbor. In recent years, strategic placement of dredged sediment in shallow water has been prioritized to allow natural processes to transport the sediment onshore and enhance coastal sediment budgets (Stevens et al., 2023). However, management of sediment resources relies on outdated sediment budgets that were primarily based on multi-decadal scale morphological change analyses conducted two decades ago (e.g., Buijsman et al., 2003). This study aims to quantify modern coastal sediment budgets adjacent to these two inlets and understand the underlying controls on morphological change to inform effective sediment management strategies.

3. Methods

3.1. Coastal morphology observations

Beach topography and nearshore bathymetry were surveyed annually between 2014 and 2023 along a series of 221 cross shore transects spaced at 100- to 1000-m intervals between Tillamook Head and Point Grenville (Fig. 1). The nested sampling scheme was designed to provide broad spatial coverage along a roughly 80-km stretch of coastline with more intensive sampling along selected locations, including the areas immediately adjacent to the maintained inlets of Grays Harbor and the Columbia River (Ruggiero et al., 2005). Data collected along the profiles extend from about 12 to 15 m water depth to landward of the primary dune crest or engineering structure, where present. The surveys were performed primarily during spring tides in the summer months of July, August, and September to characterize the morphology of the coastal landforms at a consistent time in the prominent summer-winter seasonal cycle. Bathymetric measurements were collected around high tide and topographic measurements were collected at low tide to maximize the extent of the surveys, often achieving overlap to fully characterize the cross-shore morphology on the survey lines.

Detailed seasonal variations in beach and nearshore morphology and sediment volume were analyzed for a subset of the study area using data provided in Stevens et al. (2012). That dataset, from the Southwest Washington Littoral Drift beach nourishment and monitoring study, includes 7 surveys of beach topography and nearshore bathymetry collected between July 2010 and August 2011 using similar methodology as described herein. The data were acquired to document the performance and dispersal of a beach nourishment project along Benson Beach, a 3-km long coastal section immediately north of the Columbia River inlet (Fig. 1C). These seasonal observations were used as an independent validation dataset for the developed longshore transport model in this study.

Bathymetric data were collected with personal watercraft equipped with dual-frequency global navigation satellite system (GNSS) receivers and single-beam echosounders. The echosounder systems used 200 kHz transducers with a 9 deg beam angle. Depths from the echosounders were computed using a speed-of-sound conversion derived from multiple vertical profiles of temperature and salinity collected during the surveys with a conductivity, temperature, and depth sensor. Positioning of the survey vessels was determined at 10–20 Hz using GNSS receivers operating primarily in real time kinematic mode. During post-processing, spurious soundings were removed, and the bottom profile was manually digitized where the echosounder signal processing algorithm failed to detect the bottom accurately. This was common in the surf zone where turbulence and bubbles in the water column added noise to the acoustic backscatter signal.

Topographic data were collected primarily by walking along survey lines with GNSS receivers mounted on backpacks (Ruggiero et al., 2005). Hand-held data collectors were used to log the raw data and display navigational information, allowing surveyors to walk along the

same series of survey lines as nearshore bathymetric surveys conducted during the same time period. Additional topographic data were collected in select areas using an all-terrain vehicle to constrain the elevations and along-shore extents of morphologic features.

Positions of the bathymetric and topographic measurements were differentially corrected with data from a GNSS base station placed on a nearby (typical baselines were less than 10 km) survey benchmark with known coordinates relative to the North American Datum of 1983. Differential corrections were transmitted from the GNSS base station to the survey platforms at 1 Hz intervals in real time using a UHF modem. Positions derived from differential post-processing superseded most of the positioning data from the bathymetric survey platforms and were used for the topographic platforms when real-time radio link between the base station and topographic survey platforms failed. Elevations relative to the North American Vertical Datum of 1988 (NAVD88) were computed using National Geodetic Survey Geoid12a offsets. Digital data files containing the annual bathymetric and topographic data collected between 2014 and 2023 are provided in Stevens et al. (2019); Digital files from the seasonal surveys of Benson Beach acquired between 2010 and 2011 are provided in Stevens et al. (2012).

Vertical precision of the bathymetry measurements was derived from analysis of data collected by multiple survey vessels within minutes or hours along the same transects. The methodology assumes that vertical accuracy is equivalent to vertical precision and the assumption is needed because there are no known locations on the seafloor where the elevations are fixed where the accuracy can be assessed independently. Between 2014 and 2019 a total of 30 replicate profiles were collected by at least 3 separate vessels within a short time frame and analyzed to determine the precision of the bathymetric measurements. The analysis suggested that the average vertical precision varied between 4 and 13 cm with a mean precision of 8 cm (Stevens et al., 2020). The topographic measurements would be expected to have less vertical uncertainty owing to the simplified survey system and geometry.

3.2. Sediment volume change

In order to compute changes in sediment volume along each profile, the bathymetric and topographic data were first rotated into a cross-shore coordinate system defined by the end points of the survey transects. Survey points that had positions greater than 20 m in the cross-shore direction from the target profile were discarded and the remaining points were bin-averaged at 1-m intervals. Small gaps less than 20 m along relatively smooth portions of the profiles were then filled with linear interpolation. Changes in sediment volume were quantified by summing the differences in elevation between surveys along each 1-m long segment along the profiles resulting in a volumetric change for each profile in m^3/m (Fig. 2A). Integrated volume changes in areas adjacent to the engineered inlets where survey lines were spaced less than or equal to 200 m were computed by multiplying the profile-averaged volume changes by the distances between profiles and summing these volumes to yield a total volume change within the area in m^3 (Fig. 2B). These areas generally had dimensions of around 3.5 km in the alongshore by 2.5 km in the cross shore and an area of 8,750,000 m^2. Volume changes were also calculated separately for depth zones both above and below 0 m, NAVD88, hereafter referred to as “beach” and “nearshore” areas, respectively. The NAVD88 vertical datum at this location is about 0.07 m below the mean lower low water tidal datum (NOAA Station 9439040 located inside the Columbia River inlet). Cumulative changes for each profile, depth zone, and integrated area were computed by summing the between-survey volume changes over time.

Uncertainty in the volume change measurements was estimated based on the vertical precision of the bathymetry measurements. The mean precision of each survey (8 cm) was summed in quadrature assuming that the uncertainty between surveys is independent to yield a total vertical uncertainty between surveys of 11 cm. The total uncertainty in volume change for each profile was computed by multiplying the vertical uncertainty by the length of the profile. The topographic measurements would be expected to have a higher precision, but to be conservative we did not distinguish between topographic and bathymetric measurements in our uncertainty analysis. More detailed descriptions of the volume change and uncertainty calculations can be found in Stevens et al. (2020).

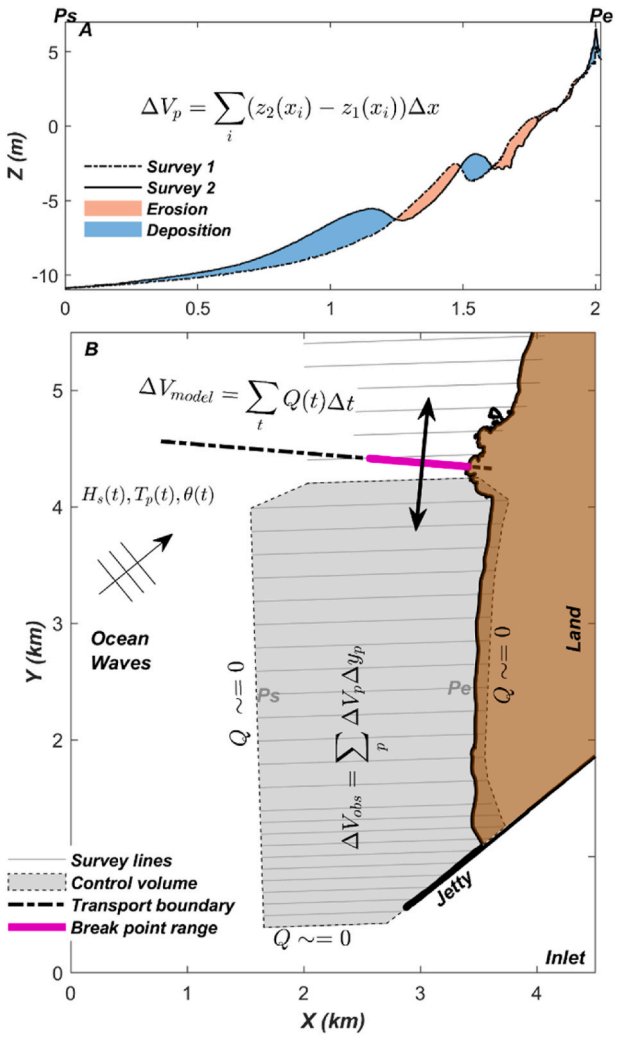


Fig. 2. Illustration of A, sediment volume change computation for an example bathymetric and topographic profile (ΔV_p), and B, schematic diagram of the box model used to compare observations of integrated volume change (ΔV_{obs}) computed for coastal areas adjacent to the engineered inlets and model predictions of volume change (ΔV_{model}). The locations of the start (Ps) and end (Pe) of the example profile shown in A are provided in B. Equations (1)–(3) describe instantaneous modeled longshore transport (Q) along the single open boundary (dashed line) of the box model.

3.3. Wave modeling

The spectral wave model SWAN (Booij et al., 1999) was applied using the Delft3D-Wave modeling system (Deltares, 2024) to simulate wave transformation and dynamics from offshore of the continental shelf (deep water) to the coastline. The model application consisted of nested grids with resolutions varying between 750 m for the largest grid to about 80 m for the two detailed grids that cover the Grays Harbor and Columbia River inlets (Fig. 1A). Model bathymetry was derived from a variety of primary datasets collected between 2004 and 2020 (Stevens et al., 2019; Gelfenbaum et al., 2015a) and existing digital elevation models (https://www.ncei.noaa.gov/maps/bathymetry/, Lower

Columbia Estuary Partnership, 2010). Wave energy was discretized into 24 frequency bins between 0.03 and 1 Hz and 72 directional bins. The model was forced on the open lateral boundaries with bulk wave parameters obtained from the ERA5 reanalysis (Hersbach et al., 2023) and on the free surface with space- and time-varying wind vectors from the High Resolution Rapid Refresh (HRRR; Dowell et al., 2022) operational forecast model with roughly 3 km spatial resolution. Wind growth and white capping were based on Komen et al. (1984). The JONSWAP bottom friction model with a coefficient of 0.038 m^2s^{-3} and wave breaking based on Battjes and Janssen (1978) with default settings (alpha = 1, gamma = 0.73) were used. SWAN was run as a stand-alone wave model neglecting the effects of wave-current interaction. We recognize the importance of wave-current interaction inside and immediately offshore of the inlets (e.g., Olabarrieta et al., 2011; Elias et al., 2012). However, the lack of wave-current interaction in our model that covers 10s of kilometers, is most likely acceptable given the limited spatial extent of wave-current interaction effects along the coastal areas adjacent to the inlets (Akan et al., 2017). Convergence criteria were set to 98 percent of cells and a maximum of 15 iterations during the simulations. The forcing conditions were updated, and wave dynamics were solved at 1-hr intervals in stationary mode between 2014 and 2023.

A second hindcast was run between July 2010 to September 2011 to simulate seasonal variations in wave climate during the Southwest Washington Littoral Drift beach nourishment and monitoring study (Stevens et al., 2012). The HRRR wind forcing was not available for this time period so an alternative downscaled wind product was used (CONUS404, Rasmussen et al., 2023). CONUS404 is a high-resolution meteorological reanalysis created by downscaling ERA5 data to a 4-km spatial resolution over the continental United States using the Weather Research and Forecasting (WRF) Model. Combined, the two hindcasts required a total of 82 days (wall clock time) to run on a variety of desktop computers. Model input files required to compute the wave hindcasts suitable for use with Delft3D-Wave version 4.04.01 are provided in Stevens et al. (2024).

3.4. Longshore transport predictions

The immersed weight longshore transport of sand (I) was estimated using the longshore component of wave power and the CERC equation (CERC, 1984):

$$I = KEsin(\theta)cos(\theta) \quad (1)$$

where K is an empirical constant and θ is the local angle between the shoreline and wave direction. E is the wave energy flux given by:

$$E = \frac{1}{16}\rho g H^2 C_g \quad (2)$$

where ρ is water density (1025 kg/m^3), g is the gravitational constant (9.81 m/s^2), H is significant wave height, and Cg is the group velocity calculated using wave numbers derived from the Newton-Raphson iteration method described in Wiberg and Sherwood (2008) and linear wave theory described in Lowe et al. (2005). Instantaneous estimates of the volumetric longshore transport rate in m^3/s (Q) were calculated using,

$$Q = \frac{I}{(\rho_s - \rho)gp} \quad (3)$$

where ρ_s is the sediment density (2650 kg/m^3) and p is the ratio of the volume of solids to the total volume sediment and is set to 0.6.

A series of 221 shore-normal transects were defined throughout the study area that extended from the coastline to the −15 m NAVD88 elevation (about 16.5 m average water depth), coincident with the survey profiles. The orientation of the transects were based on a hand digitized reference shoreline that followed the middle of the beach between the vegetated dunes and water line in aerial imagery. For each hourly time step in the wave hindcast simulations, the estimated fraction of breaking waves was interpolated onto transect locations with a cross-shore resolution of 50 m. The location of the break point, or location just outside the surf zone, varied dynamically based on the local bathymetry and wave conditions. A threshold of 0.01 of the fraction of waves breaking was used to define the time- and space-varying break point along each transect. Model output parameters, including significant wave height, peak wave period, mean wave direction, and water depth at this location, were extracted for each time step and transect and used to compute volumetric longshore transport according to equations (1)–(3).

The total cumulative volume transport was evaluated for 4 sections of coast immediately north and south of the maintained navigational inlets of Grays Harbor and the Columbia River corresponding to intensively sampled survey areas where total volume change was measured annually (Fig. 1B and C). Rock jetties define the proximal end of each of these coastline sections and longshore transport was assumed to be zero at the jetties. Sediment fluxes onshore and offshore of the measured survey areas were also assumed to be negligible. Given these assumptions, discussed in detail in section 5.2, the intensively sampled coastal segments are treated as control volumes in a simple box model (Fig. 2B) and the only open boundary where sediment is exchanged is at the distal end. We assume longshore sediment transport is the dominant process responsible for changes in sediment volume within the box. The nearest shore-normal transects to the distal ends of the control volumes were selected from the wave model (thick black lines in Fig. 1B and C), and the cumulative volumetric transport in m^3 was computed by summing the instantaneous longshore transport rates using equations (1)–(3) multiplied by the time step (3600 s). Thus, the measured sediment volume changes in the control volumes (ΔV_{obs}) are directly comparable to the cumulative longshore transport volume (ΔV_{model}) at the open boundaries of each coastal region predicted by the wave model and transport predictor (Fig. 2B) after adjusting the sign of the longshore sediment transport predictions for the coastal segments on the north sides of the inlets to account for the orientation of the jetty relative to the coastal segment (positive measured volume change/volumetric transport = deposition).

3.5. Calibration and validation of the transport predictor

Modeled longshore transport potential was calibrated to optimize agreement with the measured cumulative sediment volume change at each site adjacent to the inlets. During calibration (2014–2023), cumulative longshore transport was computed using a range of calibration coefficients (K) and wave angle bias corrections. Optimal settings for each site were selected that minimized the total root mean square error (RMSE) between measured and predicted cumulative longshore transport. Calibration of the longshore transport formula is necessary to achieve better than order of magnitude estimates of longshore transports (Splinter and Coco, 2021) due to the wide range of empirical coefficient (K) values reported in the literature for sandy beaches (0.2–1.6; Bodge and Kraus, 1991). In addition to calibration of the empirical coefficient (K), site specific wave angle bias corrections were required to accurately predict longshore sediment fluxes given the extreme sensitivity to longshore transport predictions to wave direction (Chataigner et al., 2022). Wave angle bias corrections were needed to account for errors in modeled mean wave direction as well as uncertainty in wave directions due to imprecise discretization of directional wave energy (5-degree directional bins) in the spectral wave model, and/or observational errors. Also, specification of shore normal angles was not entirely objective and were subject to some uncertainty.

The calibrated model setup was validated using independent observations of seasonal variability in sediment volume at Benson Beach during the 2010–2011 period (Stevens et al., 2012). For direct comparison of measured and modeled cumulative volume change, additional sediment was added to the model estimates to account for the 280,

000 m^3 beach nourishment that was placed on the beach during the observational study period.

4. Results

4.1. Sediment volume change and morphology observations

A total of 10 combined bathymetric and topographic surveys were performed along approximately 80 km of the Columbia River littoral cell between 2014 and 2023. Analysis of the survey data revealed significant changes in beach and nearshore sediment volume throughout the survey area (Fig. 3). Annual volumetric change between surveys for combined bathymetric and topographic profiles varied between −900 and 2050 m^3/m with a mean of 30 m^3/m. Cumulative volume changes along the coast varied between −900 and 4630 m^3/m with a mean of 270 m^3/m, suggesting a net gain of sediment of about 23 Mm^3 throughout the entire study area over the study period. The largest interannual variations in sediment volumes for combined bathymetry and topography (referred here as "total") were observed adjacent to the maintained inlets of Grays Harbor and the Columbia River (Fig. 3B). Coherent, multi-annual patterns of erosion and deposition on opposing sides of both engineered inlets were also evident in the observations (Fig. 3C and D). Between 2014 and 2019, the integrated cumulative total volume change for coastal regions on the north sides of both inlets decreased. During this time, Benson Beach on the north side of the Columbia River lost over 2 Mm^3 of sediment. Erosion at Ocean Shores on the north side of Grays Harbor peaked earlier with cumulative total erosion of about 1 Mm^3 in 2017. While the north sides of the maintained inlets eroded, significant deposition was observed on the south sides. The Westport and South Jetty regions each gained about 2 Mm^3 on the south sides of Grays Harbor and the Columbia River, respectively. After 2019, this spatially coherent pattern of erosion and deposition on the north and south sides of the inlets reversed and the north sides of the inlets accumulated sediment while the south sides of the inlets eroded resulting in little net sediment volume change over time during the study period. The cumulative beach volume changes for locations adjacent to the engineered inlets did not follow the patterns of the combined beach and nearshore system (Fig. 3E and F) and all beaches eroded measurably over the study period. While not focused on in this study, farther away from the maintained inlets, increases in cumulative total volume change were generally observed. On the north side of Willapa Bay, large amounts of sediment accumulated during the study period associated with the morphodynamics of the large unmaintained inlet.

The morphologic changes adjacent to the maintained inlets

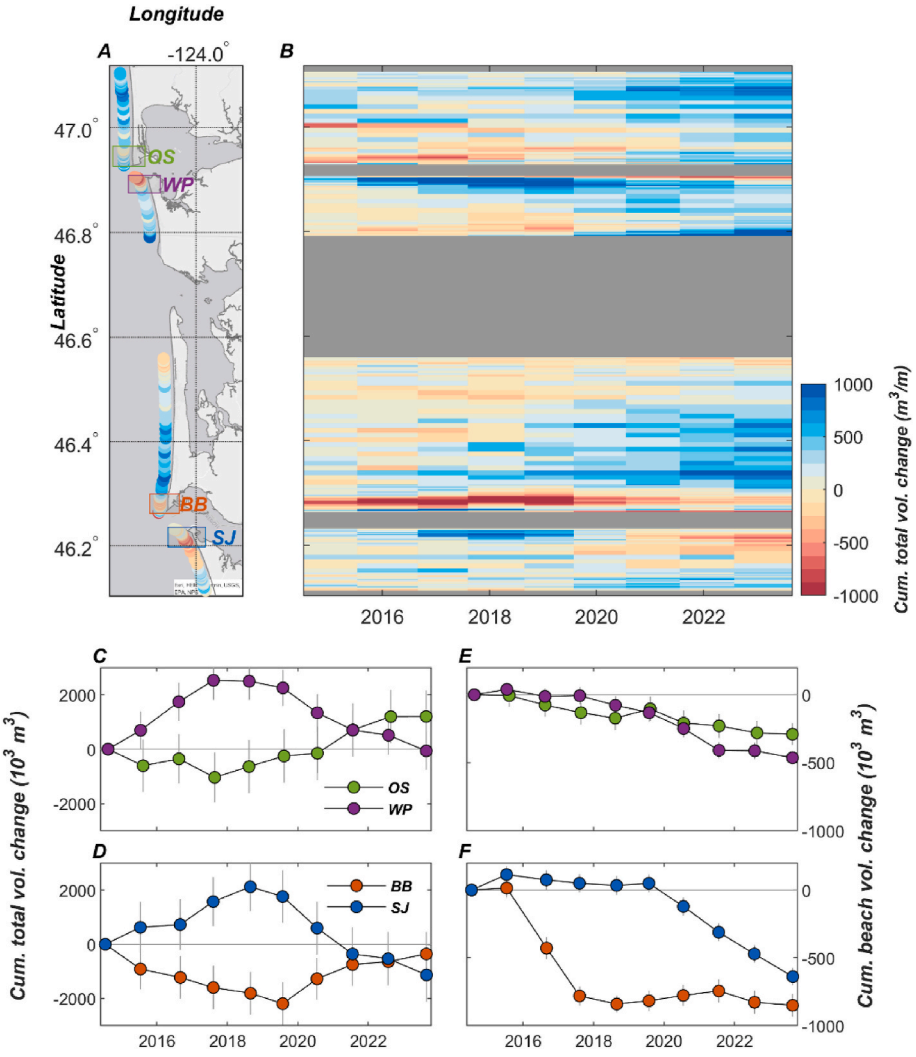


Fig. 3. Cumulative total sediment volume change for each survey profile, A, during the entire study period (2014–2023) and, B, for each annual survey. Cumulative total integrated volume change (C,D) and cumulative integrated beach volume change (E,F) are provided for the areas adjacent to the engineered inlets. The along shore extents used for integrated volume change calculations are provided in A (OS = Ocean Shores, WP = Westport, BB = Benson Beach, SJ = South Jetty). Error bars in C-F represent estimated uncertainty in cumulative sediment volume change for each region.

associated with the loss and gain of sediment volume during these two time periods (2014–2019 and 2019–2023) were spatially complex (Fig. 4). Both sediment deposition and erosion were observed throughout the cross-shore profiles. Relatively modest increases in elevation between the inner nearshore and offshore end of the survey profiles accounted for large portions of the total cumulative volume change (Fig. 4A–D). In addition, complex changes in the shallow nearshore associated with migration of prominent sandbars and beach and dune erosion resulted in large changes in elevation and volume change (Fig. 4F).

4.2. Model validation and wave forcing

Interannual variability in wave climate and longshore transport was quantified using wave model hindcasts coupled with a sediment transport predictor (CERC, 1984) during the study period. The model hindcasts of wave parameters were first validated against buoy observations at 4 locations in water depths between 24 and 183 m (Fig. 1A). Wave parameters at all of the sites were simulated with maximum root mean square errors (with root mean square errors normalized by the range of observed values in parentheses) of 0.42 m (4.4%), 2.64 s (13.5%), and 30.21 deg (8.4%) and average skill scores (Willmott, 1982) of 0.97, 0.81, and 0.78, for significant wave heights, peak wave periods, and mean wave directions, respectively (Table 1). Notably, biases of −10 and −7° were observed in the predicted wave directions for the two northern wave buoys which would have a strong influence on longshore transport predictions if calculated without wave-angle bias corrections informed by observational data.

Analysis of the hindcast data suggest that the use of a fixed water depth at the 15-m elevation contour to extract wave parameters for longshore transport calculations would lead to inaccurate characterization of the wave energy fluxes at the break point (Fig. 5). The Columbia River littoral cell is characterized by both gently sloping beaches and a highly variable wave climate. Therefore, the location of the break point can vary significantly over a wide cross-shore region depending on the wave conditions. Transformation of smaller waves that approached from the northwest occurred in much shallower water, as was typical during the summer months, than larger waves from the southwest during winter storms. For example, the wave direction just outside the surf zone at 3.5 m water depth is more than 20° different from the wave direction at the 15-m depth contour offshore for small waves from the northwest (Fig. 5F). The cross-shore locations where wave parameters were extracted depended on time-variable wave conditions to better characterize the wave conditions on the outer edge of the surf zone and improve the longshore transport calculations.

Wave energy at breaking was generally stronger on the northern sides of the maintained inlets, with deeper average break points and larger significant wave heights (Fig. 6) compared to locations to the south of the inlets. Overall, mean water depths at the break point varied between 2.9 and 4.8 m and average significant wave heights ranged between 1.4 and 2.3 m. Average wave directions at the break point generally mirrored the local shoreline orientation that varied a total of about 40 deg between −14 and 25 deg (cartesian convention, 0 = east). The largest deviations between the local shoreline angle and mean wave direction occurred in the vicinity of the Grays Harbor inlet and north of the Columbia River where the shoreline orientation changes from negative to positive (Fig. 6D).

4.3. Longshore transport

Modeled longshore transport potential accurately resolved the multi-annual patterns in erosion and deposition observed along coastal segments adjacent to the inlets (Fig. 7C). Site specific calibrations for mean wave direction to account for potential bias and the empirical constant K (eq. (1)) were required to achieve accurate longshore transport predictions (Fig. 7A and B). Mean wave angle bias corrections selected to

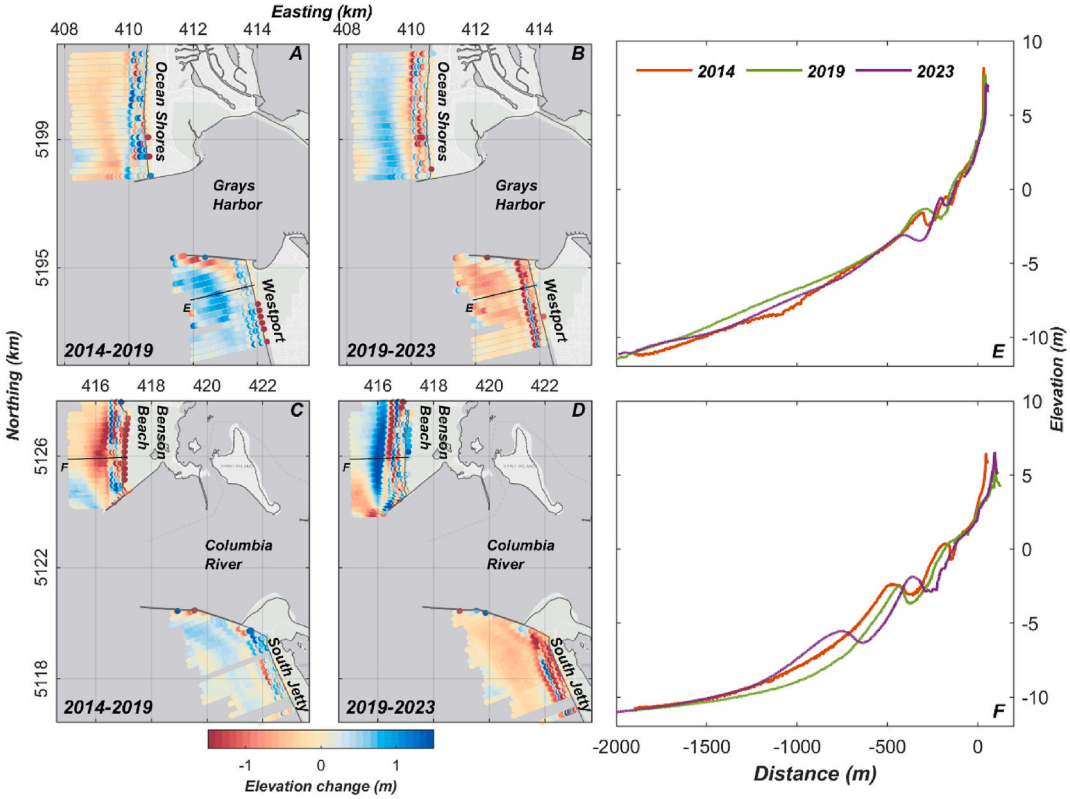


Fig. 4. Maps of measured elevation change adjacent to engineered inlets Grays Harbor (A–B) and the Columbia River (C–D) for two time periods including 2014–2019 (A,C) and 2019–2023 (B,D). Example combined bathymetric and topographic profiles from Westport and Benson Beach are shown in E-F, respectively.

Table 1
Skill metrics describing comparisons between modeled and measured bulk wave parameters at 4 buoy locations. See Fig. 1 for locations of buoys.

Agency	Site	num. obs. (n)	Significant wave height			Peak wave period			Mean wave direction		
			Bias (m)	RMSE (m)	skill	Bias (s)	RMSE (s)	skill	Bias (deg)	RMSE (deg)	skill
CDIP	179	148884	0.04	0.39	0.97	0.20	2.40	0.83	−1.72	30.21	0.77
CDIP	162	153689	0.08	0.35	0.97	0.28	2.63	0.80	2.60	22.39	0.78
NDBC	46041	64900	0.08	0.42	0.96	0.35	2.42	0.81	−10.28	29.59	0.77
CDIP	036	138446	0.09	0.37	0.96	0.30	2.64	0.79	−7.01	22.71	0.78

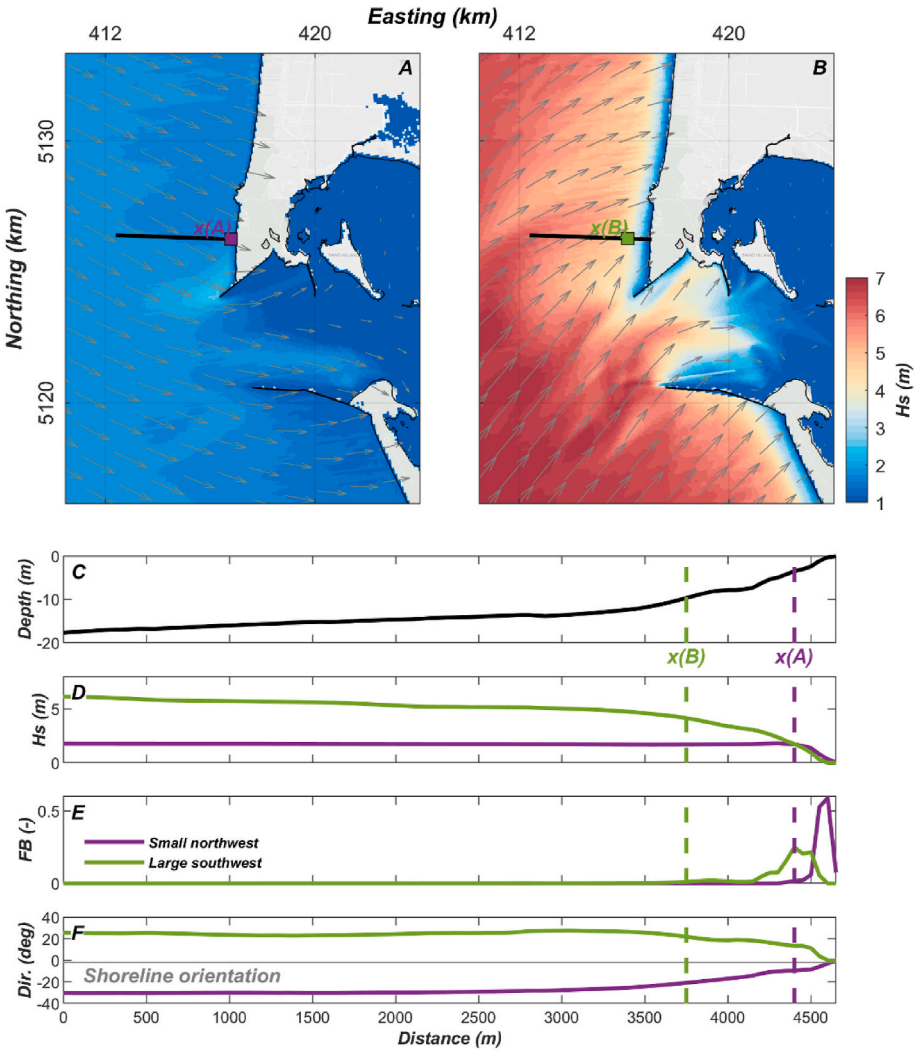


Fig. 5. Example wave heights and directions at the Columbia River for A, small waves from the northwest and B, large waves from the southwest characteristic of mild summer conditions and winter storms, respectively. Model bathymetry and parameters describing wave transformation along a shore normal transect including significant wave heights, fraction of waves breaking (FB), and mean wave direction are shown in C-F. The location of the break point for both large, x(B), and small, x (A), wave cases is shown as a square in A-B and a dashed line in C-F.

minimize error between predicted and observed cumulative longshore transport varied between 1.5 and 3° and empirical constant values varied between 0.3 and 1.1 (Table 2) for the 4 control volumes on either side of the maintained inlets (Fig. 1). After calibration, the average root-mean-square error of the predicted cumulative longshore transports was 0.32 Mm^3 or about 13% when the error is normalized by the range in observed volume change at each site.

Leveraging a finer temporal resolution dataset (Stevens et al., 2012), the calibrated transport predictor was applied to investigate seasonal changes in total sediment volume at Benson Beach (Fig. 1). During the 1-year experiment just north of the mouth of the Columbia River, 7 repeated surveys of beach topography and nearshore bathymetry performed between July 2010 and August 2011 quantified cumulative total volumetric changes ranging between 450,000 and −675,000 m^3 (Fig. 8). During the monitoring campaign, a very large wave event (significant wave height = 8.5 m) in late October caused significant changes to beach and nearshore morphology (Stevens et al., 2012) but had little impact on net total volume (Fig. 8D–F). Later in the winter and spring, Benson Beach eroded over 1 Mm^3 of sediment and a prominent outer bar disappeared (Fig. 8A–C). The present work suggests that two energetic periods (gray bars, Fig. 8D–F) with waves from the south transported sediment northward, resulting in net erosion and loss of the outer sandbar. Outside of these two energetic, erosive time periods, longshore transport was generally predicted to slowly replenish the

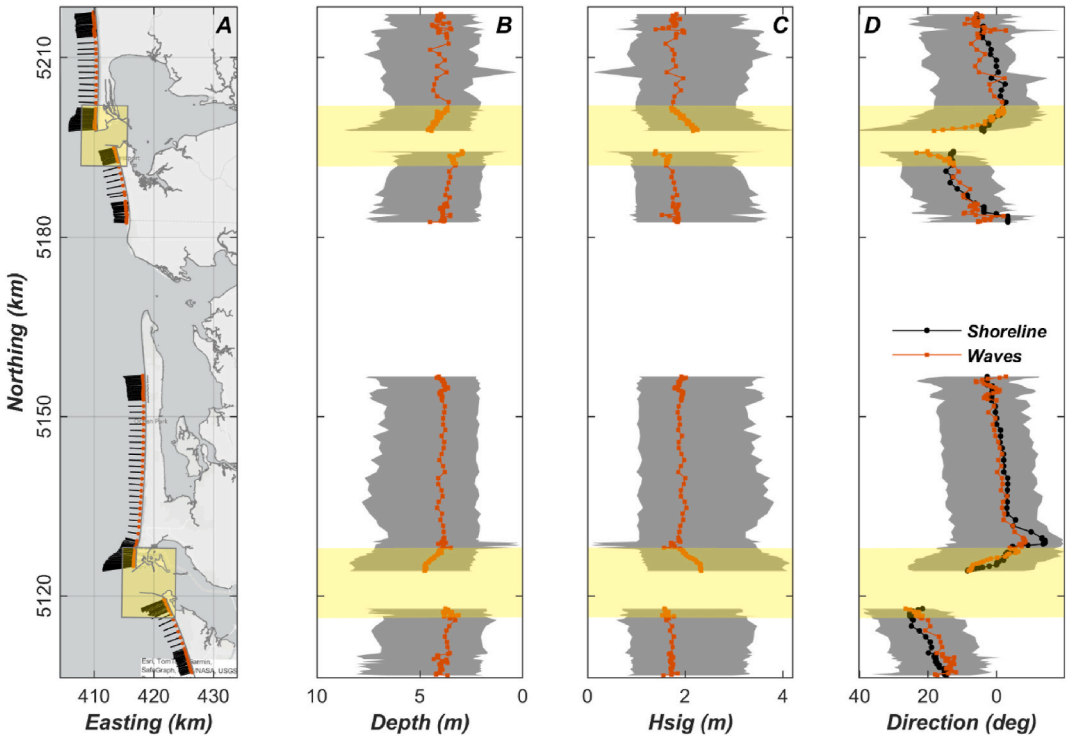


Fig. 6. Summary of alongshore variations in wave conditions during the study period (2014–2023). A, locations of shore normal model transects (black lines) and mean locations of the outer surf zone (orange dots) where wave parameters were extracted from model simulations, B, mean water depths, C, mean significant wave heights, and D, mean wave directions of waves at the outer edge of the surf zone. Panel D shows the local shoreline orientations and gray shading in B-D depicts time variability in wave parameters between the 10th and 95th percentile at each location. Yellow shading corresponds to the locations of engineered inlets and adjacent coastlines in the study area.

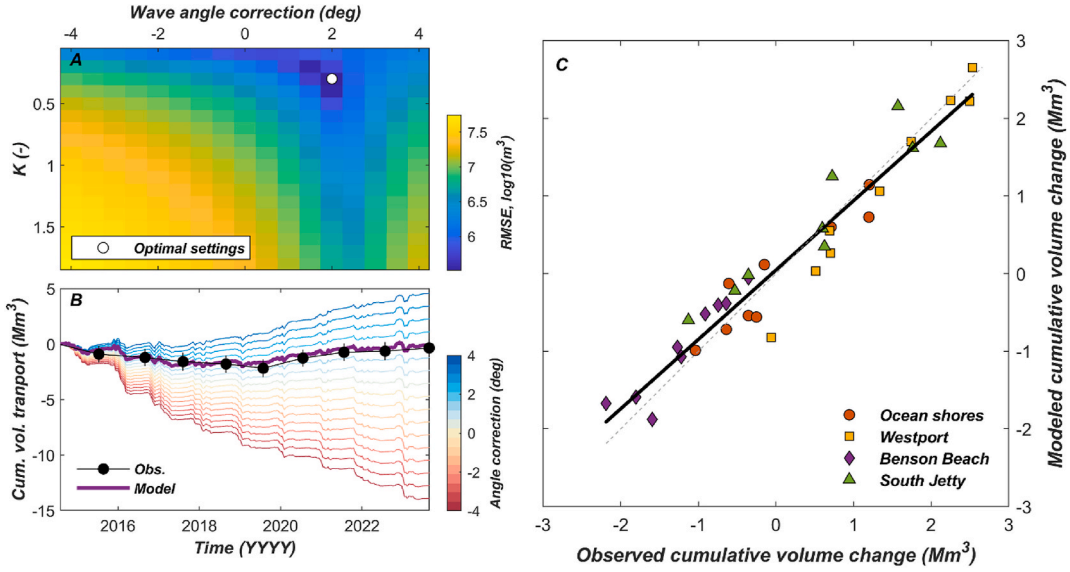


Fig. 7. Calibration of the longshore transport predictor showing, A, errors in longshore transport predictions over a range of empirical constants, K, and wave angle bias corrections for the Benson Beach region, B, sensitivity of total cumulative longshore transport to wave angle bias corrections using the optimal K value, and C, comparison of calibrated cumulative longshore transport predictions to observed volume change for all sites. Optimal settings for the Benson Beach site are denoted in A. See Table 2 for optimal settings for the other sites. Best fit (black line) and 1:1 line (gray dashed line) is shown in C.

supply of sand to Benson Beach with sediment from the north.

The seasonal data from Benson Beach were not used for model calibration and therefore provide an independent opportunity to validate the predictive capacity of the transport formula. Root mean square error between modeled and predicted total volume change for the seasonal data was 131,000 m^3 or about 12% when normalized by the range of observed volume change. This is similar to the accuracy of annual volume change predictions (average = 13% for all sites, 15% for Benson Beach).

Table 2
Optimized values for computing longshore sediment flux, root mean squared error (RMSE), root mean square error normalized by observed range in volume change (NRMSE), and estimated uncertainty in measured sediment volume change for each control volume inlet region. See Fig. 1 for locations of control volumes and transects used for longshore transport calculations.

Inlet	Location	Wave angle correction (deg)	K	RMSE (Mm3)	NRMSE (%)	Vol. change uncertainty (Mm3)
Grays Harbor	Ocean Shores	3	0.4	0.26	11	0.96
Grays Harbor	Westport	2.5	1.1	0.34	13	0.71
Columbia River	Benson Beach	2	0.3	0.32	15	0.81
Columbia River	South Jetty	1.5	0.8	0.35	12	0.99

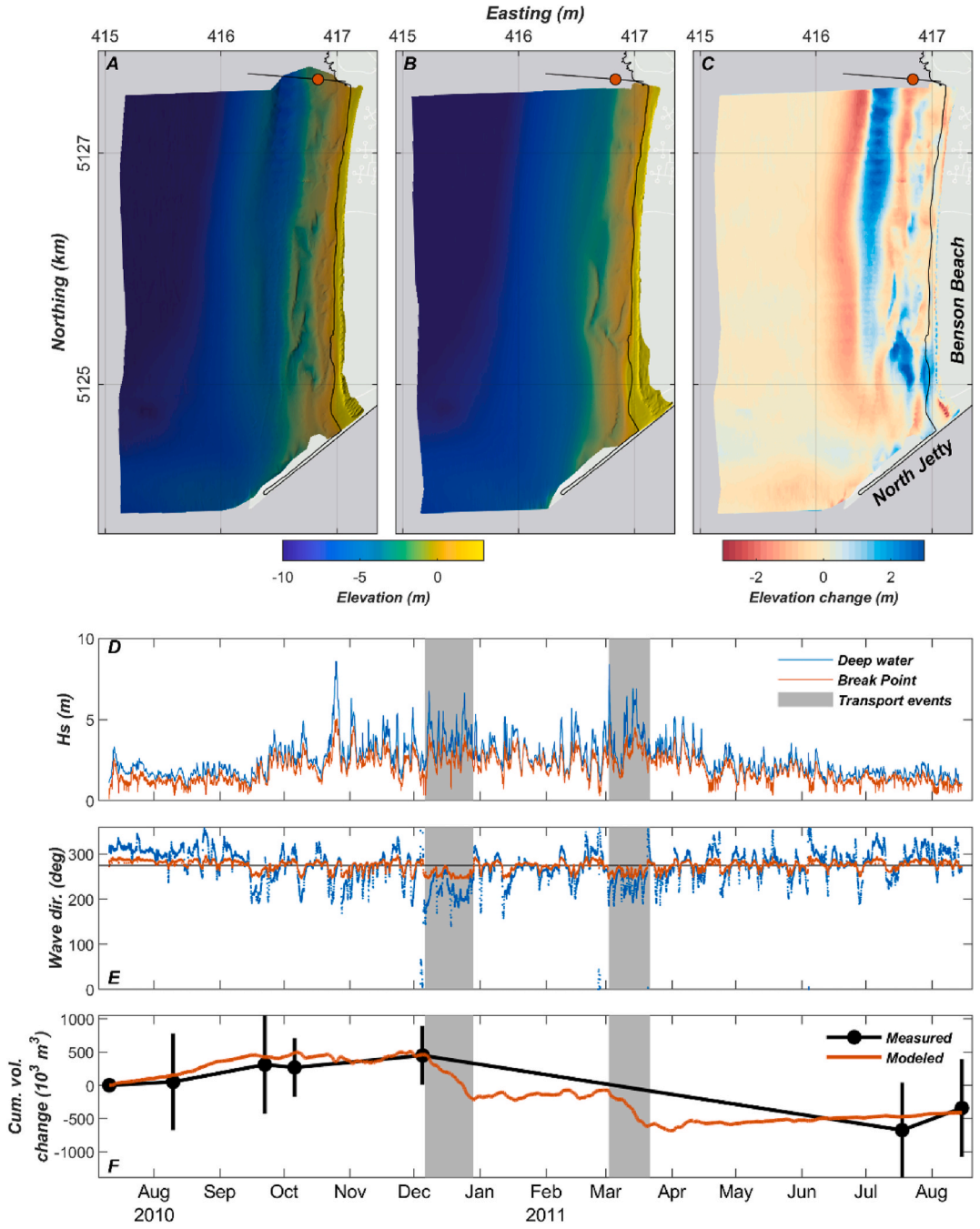


Fig. 8. Validation of the calibrated longshore transport predictor using seasonal observations of total volume change at Benson Beach. Elevation of beach and nearshore in, A, July 2010 and B, August 2011. C, Difference in elevation between August 2011 and July 2010. Time series showing D, significant wave heights, E, mean wave directions for deep water and at the break point, and F, measured (black line) and modeled cumulative volume change (red line). Deep water wave conditions are provided at the location of CDIP buoy 179 (see Fig. 1 for location of buoy). Black transects and orange dots in A-C show the extent of the surf zone and mean location of the break point used for longshore transport calculations, respectively. Black line in E is the local shoreline orientation and gray shading in D-F denotes time periods of northward transport and loss of sediment volume from the beach and nearshore.

4.4. Climate forcing

Observed beach and nearshore volume changes and associated wave forcings were compared with the El Niño/Southern Oscillation index version 3.4 (ONI; https://www.cpc.ncep.noaa.gov/data/indices/oni.ascii.txt) and the Pacific Decadal Oscillation index (PDO; https://www.ncei.noaa.gov/pub/data/cmb/ersst/v5/index/ersst.v5.pdo.dat) known to affect environmental conditions throughout the Pacific Basin at interannual to multidecadal time scales, respectively. Large positive El Niño index values during the 2015/2016 winter, indicating strong El Niño conditions, resulted in increased wave heights (Fig. 9C) and exceptionally large northward longshore transport relative to other years (Fig. 9E). However, other years, not associated with a strong El Niño event, including 2014/2015 and 2016/2017, also produced northward sediment transport (Fig. 9E). The PDO index reversed from a positive phase at the beginning of the study to a negative phase in 2019 with neutral conditions in between. Years with positive or neutral PDO phases were associated with northerly transport and erosion of the beaches on the north sides of the inlets while the negative phases were associated with transport to the south (Fig. 9E). Regardless of the phases of the climate indices, the annual patterns of longshore transport resulting in erosion or deposition along the coastal segments were dominated by relatively short intense periods of northward transport in the (high-energy) winter that interrupted more gradual southward transport during much of the year (calm conditions). Years with positive PDO contained time periods with more persistent northward directed wave energy flux that controlled the overall balance of longshore transports during the year.

5. Discussion

5.1. Observations of coastal change

Despite the dynamic nature of coastal morphology and its importance to coastal applications, long-term observations that quantify changes in both subaerial beach and nearshore morphology are uncommon (but see Ludka et al., 2019; Turner et al., 2016; Bertin et al., 2022; McCarroll et al., 2023). The observational campaign described and analyzed for this study consisted of 221 bathymetric and topographic profiles collected annually between 2014 and 2023 along roughly 80 km of modally dissipative barred beaches (Ruggiero et al., 2005). The relatively unique characteristics of the dissipative, mostly prograding beaches (Ruggiero et al., 2016) characterized by multiple pronounced sandbars included in this study provides excellent opportunities to test numerical models (Cohn and Ruggiero, 2016; Splinter et al., 2018; Saunders et al., 2024) and assess the performance of new methodologies for coastal change detection (e.g., Graffin et al., 2023). It also provides a critical baseline dataset for understanding the coastal dynamics and morphological context of the greater northeast Pacific coastline. Here, analysis of this dataset focused on beach and nearshore sediment volume change adjacent to two engineered inlets (Figs. 3–4), Grays Harbor and the Columbia River located about 75 km apart (Fig. 1). Observations of beach and nearshore morphology and sediment volume change adjacent to the two inlets revealed spatially coherent patterns of erosion and deposition that persisted over several years and then reversed. Given the proximity of these beaches to deep water jetties and associated disruptions to longshore transport, we hypothesized that the observed changes in coastal morphology represented a longshore coherent transport pattern (Ibaceta et al., 2023) resulting in rotation of the beach planform (e.g., Ranasinghe et al., 2004) in response to

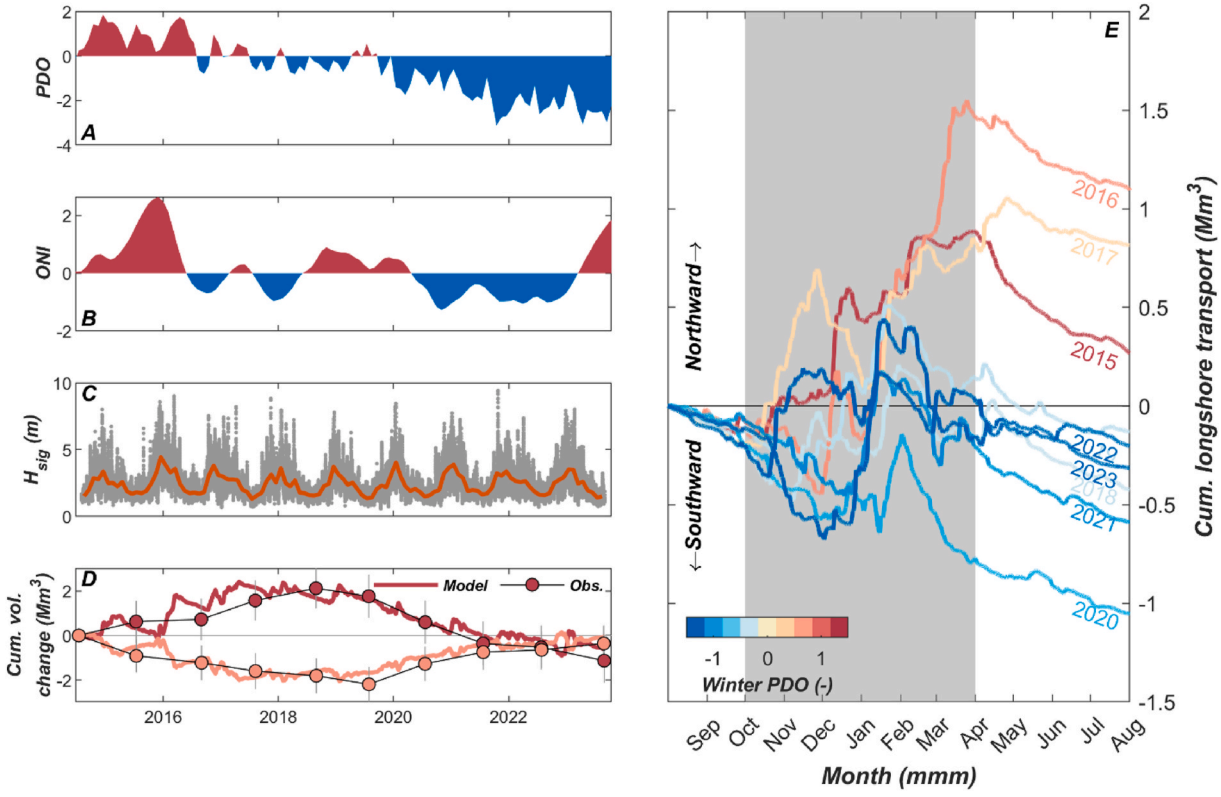


Fig. 9. Time series of A, Pacific Decadal Oscillation index (PDO), B, seasonal El Niño/Southern Oscillation index (ONI), C, hourly (gray dots) and monthly averaged (orange line) modeled wave heights, D, modeled (thick lines) and measured (thin black lines with error bars) cumulative volume change at South Jetty (red) and Benson Beach (orange), E, annual cumulative longshore transport at South Jetty for each year during the study colored by the mean PDO index value during the fall and winter months of October through March (gray shading). Year labels in E denote the year that the record ends (that is, 2015/2016 = 2016).

large-scale, multi-annual variability in the wave climate. This hypothesis was tested using a combination of numerical modeling to resolve nearshore wave dynamics and a simple longshore transport predictor.

The morphologic changes adjacent to the maintained inlets were spatially complex and showed significant cross-shore variability (Fig. 4). For instance, over 2 Mm^3 of net sediment deposition was observed between 2014 and 2019 along Westport on the south side of Grays Harbor (Fig. 3C) with a relatively thin deposit of sediment that extended from about −5 m seaward to the lower shoreface at the offshore extent of the survey area (Fig. 4A–E). At the same time of this large increase in nearshore sediment volume, portions of this coastline eroded, the dune crest moved landward over 20 m, and its height reduced by over 1 m (Fig. 4E), resulting in net erosion of 130,000 m^3 of sediment from the beach (Fig. 3E). This heterogeneous morphodynamic development with volume change that was dominated by the subaqueous portion of the active profile is not uncommon (e.g., Gelfenbaum et al., 2015b; Harley et al., 2022) and highlights the challenge of solely relying on subaerial observations to understand coastal sediment budgets or to calibrate and validate models of coastal change (e.g., Antolinez et al., 2018) for sediment management applications.

5.2. Model performance and limitations

Accurate predictions of longshore sediment transport fluxes have been a longstanding goal of coastal scientists (Komar and Inman, 1970). Application of longshore transport predictors such as the CERC equation (CERC, 1984) in combination with wave hindcasts and forecasts is a common approach to investigate coastal change over a variety of temporal and spatial scales (Ruggiero et al., 2010b; Adams et al., 2011; Anderson et al., 2018; Ludka et al., 2023). Model predictions of longshore transport using this relatively simple approach are subject to many sources of uncertainty, including errors in the wave parameters used as model input, uncertainty in calibration coefficients (e.g., K in eq. (1)), and assumptions about exchange of sediment at the model boundaries (e.g., Ruggiero et al., 2010b). Previous studies have often utilized a fixed water depth (typically 10 m, e.g., Kaul et al., 2024) to represent the wave parameters that are used in longshore transport predictions, neglecting the dynamic response of varying wave conditions to the local bathymetry (Fig. 5). Our model results indicate that the depth of the outermost breaking waves varied between about 1.5 and 16 m with a mean of roughly 3 m (mean 95th percentile along the coast was about 7 m; Fig. 6B), much shallower than is usually selected for longshore transport calculations despite the high wave energy at our study site. This suggests that use of wave conditions that are based on time- and space-varying conditions more accurately resolve the wave dynamics at the break point and improve longshore transport calculations.

The changes in observed beach and nearshore sediment volume adjacent to two engineered inlets provide direct comparisons to predicted longshore sediment fluxes assuming limited pathways for sediment exchange outside the measurement areas, or control volumes. Although our comprehensive measurements integrate over a vast majority of the active profile, sediment exported from the control volumes via landward transport into the dunes (e.g., Cohn et al., 2018), sediment bypassing the rock jetties, and sediment exchanged with the lower shoreface during storms (e.g., Harley et al., 2022) or by strategic nearshore placements of dredge material in the nearshore (Stevens et al., 2023) were all assumed to be negligible in our box model (Fig. 2B). We acknowledge these transport pathways are likely to occur, but argue they were small relative to the large longshore sediment fluxes along the open lateral boundaries (see Fig. 1B and C for open boundary locations). This assumption is supported by Ruggiero et al. (2010b), who found that gradients in longshore transport accounted for 80% of the decadal scale variability in shoreline position along the Long Beach peninsula north of Benson Beach. In addition, time-invariant unmeasured fluxes would be absorbed into the calibration coefficients (K) during model optimization. These unmeasured fluxes likely contributed to the differences in computed K values among the north and south sides of the inlets (Table 2). Alongshore variations in sediment mineralogy and grain-size (Li and Komar, 1992; Ruggiero et al., 2005) not included in the model simulations may also have influenced variable calibration coefficients. The remarkable performance of the relatively simple model (Fig. 7C; Fig. 8F) suggests that the above assumptions are well justified for the study site.

Longshore transport predictions using Eq. (1) are extremely sensitive to small changes in mean wave angle (Fig. 7B; Chataigner et al., 2022). Overall, the maximum wave angle bias correction (3°) was much less than the bias in modeled mean wave direction at buoy site 46041 offshore of Ocean Shores (Table 2). Without observational data to inform wave bias corrections and calibration coefficients, accurate predictions of longshore transport would have been impossible. After calibration of the longshore transport predictor, simulated sediment fluxes were highly accurate compared to annual observations of cumulative sediment volume change with an average normalized RMSE error of 13% for all of the sites investigated (Fig. 7; Table 2). Unlike several other approaches that require time variable fitting of model calibration parameters (e.g., Vitousek et al., 2017; Ibaceta et al., 2022), no temporal adjustments to the calibration coefficients or wave bias corrections were required for robust estimates of the longshore transports for the entire 9-yr observation period. While the exceptional fit is encouraging, these accuracies represent a best fit between observed volume change and the longshore component of wave energy flux during calibration. Validation of the transport predictor using seasonal observations of sediment volume change not used in the model calibration confirmed the general applicability of the approach (Fig. 8F). Errors in cumulative longshore transport for the validation data were equivalent (12%) to the calibration results when the transport predictor was applied to independent seasonal observations at Benson Beach, suggesting the model was skilled at predicting seasonal and likely event-scale longshore transport fluxes as well as the multi-annual trends.

5.3. Temporal patterns of longshore transport and climate forcing

The robust model framework presented here allows for characterization and quantification of the dominant temporal forcing responsible for coastal change not captured with the annual observations. Seasonal variability in the wave forcing (Fig. 1A) and associated magnitude and direction of longshore transport was dominated by the presence of relatively short (~1 month) time intervals of elevated wave energy, or storm sequences, with northward transport in the winter that interrupted more gradual and consistent southward transport throughout the spring and summer (Figs. 8F and 9E). Years devoid of storm sequences with northward transport or those with relatively weak northward transport events as in 2020 resulted in net southward transport (Fig. 9E) and deposition of sediment on the north side of the engineered inlets (Fig. 9D) during the year. Our observations and modeling support the recently recognized importance of relatively short storm sequences on coastal sediment budgets suggested by Harley et al. (2022). We, however, emphasize the role of wave direction during the storm sequence and subsequent net longshore transport as a primary driver of nearshore volumetric change. For example, during the 2010 seasonal observations at Benson Beach, a very large wave event with wave direction orthogonal to the coastline at the beginning of October (Fig. 8D) caused significant cross-shore transport and morphology change (Stevens et al., 2012), but no measurable net volume change (Fig. 8F). More impactful on the total sediment budget were more modest storms with northerly directed wave energy later in the winter that caused over 1 Mm^3 of sediment loss and major changes to the large subaqueous bar system (Fig. 8; Stevens et al., 2012; Splinter et al., 2018).

Changes in coastal morphology at sites around the world have recently been linked with large scale climate indices using both detailed morphology observations (e.g., Wiggins et al., 2019; Masselink et al., 2023) and remotely sensed shoreline positions (Vos et al., 2023). Ocean

facing beaches along the eastern North Pacific where our study area is located respond to climate variability associated with the El Niño/Southern Oscillation (Barnard et al., 2017; Vos et al., 2023). During El Niño winters, two primary effects are responsible for changes in coastal morphology: 1) elevated wave energy and water levels result in enhanced cross-shore transport between the subaerial beach and nearshore and 2) changes in wave direction driving coherent longshore transport patterns that result in planform rotation (Ranasinghe et al., 2004; Ruggiero et al., 2013). PDO phases have been tied to similar patterns in wave energy flux anomalies as El Niño, with warm (cool) Pacific Decadal Oscillation phases correlating with increased (decreased) wave energy in the northeast Pacific (Casas-Prat et al., 2024). The monitoring period that encompasses this study included the El Niño winter of 2015/2016, one of the strongest in recorded history (Barnard et al., 2017). Between the summers of 2015 and 2016, analysis of sediment volume change for the subaerial beach (Fig. 3E and F) did not indicate widespread severe erosion despite enhanced winter erosion reported by Barnard et al. (2017). This lack of response in our annual observations was likely due in part to the late summer timing of the surveys failing to capture the maximum extent of beach erosion during the winter and suggests a rapid recovery of the beaches the following spring and early summer (e.g., Cohn et al., 2018). In addition, changes in longshore transport associated with the 2015/2016 El Niño were likely less dramatic because the wave direction anomaly in our study region was not particularly strong for this event (Barnard et al., 2017).

Multi-annual temporal variability was prominent in our observations of beach and nearshore sediment volume (Figs. 3, 4 and 9). The reversal in the multi-annual, regionally coherent trends in erosion and deposition coincided with a switch in sign of the Pacific Decadal Oscillation (PDO) climate index (Fig. 9). During the warm phase (positive) of the PDO, stronger and more frequent storm sequences from the south resulted in net northward transport and deposition of sediment on the south side of the engineered inlets. The transport direction reversed between 2017 and 2019 and the opposite pattern has persisted for the duration of the monitoring period corresponding to a cool phase (negative) PDO. Over longer time scales, Anderson et al. (2018) noted a similar correlation between phases of the PDO and longshore transport directions predicted by model simulations. Simulated longshore transports exhibited a dramatic change in direction around 1980 when the PDO shifted from a cold phase to a warm phase. This switch in PDO altered basin scale wind stress patterns and significantly altered regional trends in sea level rise (Bromirski et al., 2011). Northward (southward) directed longshore transport during the warm (cool) phase of the PDO is consistent with wind stress anomalies along eastern north Pacific derived from multiple regression of the PDO and model reanalysis of basin scale winds (cf. Fig. 8 in Moon et al., 2013). Combined, these analyses suggest that multi-decadal variability in large scale atmospheric and oceanographic processes, which are at least partially described by the PDO index play an important role in the dynamic balance of alongshore wave energy flux and resulting longshore transport for beaches along the eastern North Pacific.

5.4. Implications for sediment management

The ability to predict volumetric change along beaches adjacent to maintained inlets has obvious implications for regional sediment management. The U.S. Army Corps of Engineers maintains both Grays Harbor and the Columbia River with long rock jetties and annual maintenance dredging of the inlet channels. In recent years, strategic placement of dredged sediment in the active nearshore has been prioritized to minimize loss of sediment from the littoral system. At the mouth of the Columbia River, a majority of the 2–4 Mm^3 of sediment dredged annually from the navigation channel is placed within a network of permitted placement sites located both north and south of the inlet. The management approach is designed to allow natural processes to redistribute sediment from its placement location to preserve habitat for benthic ecosystems (Roegner et al., 2021), avoid excessive sediment deposition leading to wave amplification and associated navigational hazards, and enhance sediment supply to adjacent shorelines. In combination with detailed hydrodynamic and sediment transport models used to identify effective placement sites (Stevens et al., 2023), model predictions of longshore transport and cumulative volume change using the model framework developed in this study can be used to provide timely information to decision-makers to optimize placement of the dredge material and target specific areas experiencing sediment deficits and associated coastal erosion hazards.

6. Conclusions

Bathymetric and topographic surveys performed annually between 2014 and 2023 were used to quantify beach and nearshore morphology and sediment volume change along an 80-km stretch of wave dominated coastline in the northeast Pacific Ocean. The observations revealed distinct multi-annual patterns in sediment volume change for the coasts adjacent to two engineered inlets within the study area. Opposing sediment erosion and deposition on either side of the engineered inlets that persisted for several years and then reversed suggested a longshore coherent transport pattern and planform rotation of the coastal system in response to large scale wave climate variability. A numerical modeling application was developed to predict nearshore wave dynamics and, in combination with a longshore sediment transport predictor and simple box model, explain changes in sediment volume along the coast.

The model simulations confirm that reversals in longshore sediment transport direction were primarily responsible for the observed changes in sediment volume for the coasts adjacent to the engineered inlets. Multi-annual variability in the wave climate, in particular wave direction, affected the dynamic balance of longshore transport and dominated the observed patterns in sediment dynamics. The multi-annual patterns in wave climate, longshore transport, and coastal morphology change appears to be part of a longer (multi-decadal) trend driven, at least in part, by the Pacific Decadal Oscillation. Improved understanding of the temporal variability and processes responsible for changes in coastal morphology and sediment budgets are essential to inform effective management of sediment resources, particularly in the vicinity of engineered inlets where jetties constrain longshore sediment transport pathways.

Data availability

Bathymetric and topographic data presented in this study are available in Stevens et al. (2012, 2019). Spectral wave model input files suitable for use with Delft3D-Wave version 4.04.01 (Deltares, 2024) and time-series of wave parameters used for longshore sediment transport calculations are provided in Stevens et al. (2024).

CRediT authorship contribution statement

Andrew W. Stevens: Writing – review & editing, Writing – original draft, Visualization, Project administration, Methodology, Investigation, Funding acquisition, Formal analysis, Data curation, Conceptualization. **Peter Ruggiero:** Writing – review & editing, Resources, Methodology, Investigation, Data curation, Conceptualization. **Kai A. Parker:** Writing – review & editing, Investigation, Data curation. **Sean Vitousek:** Writing – review & editing, Methodology, Investigation, Formal analysis. **Guy Gelfenbaum:** Writing – review & editing, Investigation, Conceptualization. **George M. Kaminsky:** Writing – review & editing, Resources, Methodology, Investigation, Data curation, Conceptualization.

Declaration of competing interest

The authors declare that they have no known competing financial interests or personal relationships that could have appeared to influence the work reported in this paper.

Acknowledgments

Funding for this work was provided by the U.S. Army Corps of Engineers Portland District, U.S. Geological Survey Coastal and Marine Hazards and Resources Program, the Northwest Association of Networked Ocean Observing Systems (NOAA-IOOS Award NA21NOS0120093), and the Cascadia Coastlines and Peoples Hazards Research Hub, an NSF Coastlines and People Large-Scale Hub (NSF award number 2103713). We thank Hans (Rod) Moritz, James McMillan, Samantha Lynch, and Julia Keiter (USACE) for supporting coastal monitoring at the mouth of the Columbia River. Coastal surveys were made possible by the tireless efforts of the Nearshore Allstars, in particular, Jeff Wood, Meredith Leung, Katy Serafin, Dylan Anderson, Paige Hovenga, Nick Cohn, Mohsen Taherkhani (Oregon State), Tim Elfers, Jackson Currie, Cordell Johnson, Josh Logan (U.S. Geological Survey), Heather Weiner, Amanda Hacking, Diana McCandless, and Hannah Drummond (Washington State Department of Ecology). Jon Warrick (USGS) and two anonymous reviewers improved an earlier version of this manuscript. Any use of trade, firm, or product names is for descriptive purposes only and does not imply endorsement by the U. S. Government.

References

Adams, P.N., Inman, D.L., Lovering, J.L., 2011. Effects of climate change and wave direction on longshore sediment transport patterns in Southern California. Climatic Change 109 (Suppl. 1), S211–S228. https://doi.org/10.1007/s10584-011-0317-0.

Akan, C., Moghimi, S., Ozkan-Haller, H.T., Osborne, J., Kurapov, A., 2017. On the dynamics of the Mouth of the Columbia River: results from a three-dimensional fully coupled wave-current interaction model. J. Geophys. Res.: Oceans 122, 5218–5236.

Allan, J.C., Gabel, L.L., 2016. Monitoring the response and efficacy of a dynamic revetment constructed adjacent to the Columbia River South Jetty, clatsop county, Oregon. Oregon Dep. Geol. Miner. Ind. Open-File Rep. 50. O-16-07.

Anderson, D., Ruggiero, P., Antolinez, J.A.A., Mendez, F.J., Allan, J., 2018. A climate index optimized for longshore sediment transport reveals interannual and multidecadal littoral cell rotations. J. Geophys. Res.: Earth Surf. 123, 1958–1981. https://doi.org/10.1029/2018JF004689.

Antolinez, J.A.A., Mendez, F.J., Anderson, D., Ruggiero, P., Kaminsky, G.M., 2018. Predicting climate-driven coastlines with a simple and efficient multi-scale model. J. Geophys. Res.: Earth Surf. 124, 1596–1624. https://doi.org/10.1029/2018JF004790.

Barnard, P.L., Schoellhamer, D.H., Jaffe, B.E., McKee, L.J., 2013. Sediment transport in the San Francisco Bay coastal system: an overview. Mar. Geol. 345, 3–17.

Barnard, P.L., Hoover, D., Hubbard, D.M., Snyder, A., Ludka, B.C., Allan, J., et al., 2017. Extreme oceanographic forcing and coastal response due to the 2015-2016 El Niño. Nat. Commun. 8, 14365. https://doi.org/10.1038/ncomms14365.

Battjes, J., Janssen, J., 1978. Energy loss and setup due to breaking of random waves. Coast. Eng. Proc. 1 (16), 32. https://doi.org/10.9753/icce.v16.32.

Bayle, P.M., Kaminsky, G.M., Blenkinsopp, C.E., Weiner, H.M., Cottrell, D., 2021. Behaviour and performance of a dynamic cobble berm revetment during a spring tidal cycle in North Cove, Washington State, USA. Coast. Eng. 167, 103898.

Bergsma, E.W.J., Almar, R., Rolland, A., Binet, R., Brodie, K.L., Bak, A.S., 2021. Coastal morphology from space: a showcase of monitoring the topography-bathymetry continuum. Rem. Sens. Environ. 261, 112469. https://doi.org/10.1016/j.rse.2021.112469.

Bertin, S., Floc'h, F., Le Dantec, N., Jaud, M., Cancouet, R., Franzetti, M., et al., 2022. A long-term dataset of topography and nearshore bathymetry at the macrotidal pocket beach of Porsmilin, France. Sci. Data 9, 79. https://doi.org/10.1038/s41597-022-01170-3.

Bodge, K.R., Kraus, N.C., 1991. Critical examination of longshore transport rate magnitude. Proc. Coast. Sediments 1991, 139–155.

Booij, N., Ris, R.C., Holthuijsen, L.H., 1999. A third generation wave model for coastal regions, Part I—model description and validation. J. Geophys. Res. 104, 7649–7666.

Bromirski, P.D., Miller, A.J., Flick, R.E., Auad, G., 2011. Dynamical suppression of sea level rise along the Pacific coast of North America: indications for imminent acceleration. J. Geophys. Res. 116, C07005. https://doi.org/10.1029/2010JC006759.

Buijsman, M.C., Sherwood, C.R., Gibbs, A.E., Gelfenbaum, G., Kaminsky, G., Ruggiero, P., Franklin, J., 2003. Regional sediment budget of the Columbia River littoral cell, USA, analysis of bathymetric- and topographic-volume change. U.S. Geol. Surv. Rep. 02-281 167. http://pubs.usgs.gov/of/2002/of02-281/.

Casas-Prat, M., Hemer, M.A., Dodet, G., Morim, J., Wang, X.L., Mori, N., et al., 2024. Wind-wave climate changes and their impacts. Nat. Rev. Earth Environ. 5, 23–42. https://doi.org/10.1038/s43017-023-00502-0.

CERC, 1984. Shore protection manual. Dep. Army Waterw. Exp. Stn. Corps Eng. 1.

Chataigner, T., Yates, M.L., Le Dantec, N., Harley, M.D., Splinter, K.D., Goutal, N., 2022. Sensitivity of a one-line longshore shoreline change model to the mean wave direction. Coast. Eng. 172, 104025. https://doi.org/10.1016/j.coastaleng.2021.104025.

Cohn, N., Ruggiero, P., 2016. The influence of seasonal to interannual nearshore profile variability on extreme water levels: modeling extreme runup on dissipative beaches. Coast. Eng. 115, 79–92.

Cohn, N., Ruggiero, R., de Vries, S., Kaminsky, G.M., 2018. New insights on coastal foredune growth: the relative contributions of marine and aeolian processes. Geophys. Res. Lett. 45, 4965–4973. https://doi.org/10.1029/2018GL077836.

Deltares, 2024. Delft3d 4 suite version 4.04.01. Retrieved from. https://download.deltares.nl/delft3d-4-suite.

Di Leonardo, D., Ruggiero, P., 2015. Regional scale sandbar variability: observations from the U.S. Pacific Northwest. Continent. Shelf Res. 95, 74–88. https://doi.org/10.1016/j.csr.2014.12.012i.

Dowell, D.C., Alexander, C.R., James, E.P., Weygandt, S., Benjamin, S.G., Manikin, G.S., et al., 2022. The high-resolution rapid Refresh (HRRR), an hourly updating convection-allowing forecast model. Part I: motivation and system description. Weather Forecast. 37, 1371–1395. https://doi.org/10.1175/WAF-D-21-0151.1.

Elias, E.P.L., Gelfenbaum, G., Wan der Westhuysen, A.J., 2012. Validation of a coupled wave-flow model in a high-energy setting: the mouth of the Columbia River. J. Geophys. Res. 117, C09011.

Elias, E.P.L., van der Spek, A.J.F., Pearson, S.G., Cleveringa, J., 2019. Understanding sediment bypassing processes through analysis of high-frequency observations of Ameland Inlet, The Netherlands. Mar. Geol. 415, 105956. https://doi.org/10.1016/j.margeo.2019.06.001.

Gelfenbaum, G., Kaminsky, G.M., 2010. Large-scale coastal change in the Columbia River littoral cell: an overview. Mar. Geol. 273, 1–10. https://doi.org/10.1016/j.margeo.2010.02.007.

Gelfenbaum, G.R., Finlayson, D.P., Dartnell, P., Carlson, E., Stevens, A.W., 2015a. Bathymetry and backscatter from 2013 interferometric swath bathymetry systems survey of Columbia River Mouth, Oregon and Washington. U.S. Geol. Surv. Data Release. https://doi.org/10.5066/F7T72FHB.

Gelfenbaum, G., Stevens, A.W., Miller, I., Warrick, J.A., Ogston, A.S., Eidam, E., 2015b. Large-scale dam removal on the Elwha River, Washington, USA: coastal geomorphic change. Geomorphology 246, 649–668. https://doi.org/10.1016/j.geomorph.2015.01.002.

Graffin, M., Taherkhani, M., Leung, M., Vitousek, S., Kaminsky, G., Ruggiero, P., 2023. Monitoring interdecadal coastal change along dissipative beaches via satellite imagery at regional scale. Camb. Prisms: Coast. Futures 1 (e42), 1–14.

Harley, M.D., Masselink, G., Ruiz de Alegria-Arzaburu, A., Valiente, N.G., Scott, T., 2022. Single extreme storm sequence can offset decades of shoreline retreat projected to result from sea-level rise. Nature: Commun. Earth Environ. 3, 112. https://doi.org/10.1038/s43247-022-00437-2.

Hersbach, H., Bell, B., Berrisford, P., Biavati, G., Horányi, A., Muñoz Sabater, J., et al., 2023. ERA5 hourly data on single levels from 1940 to present. Copernicus Clim. Change Serv. (C3S) Clim. Data Store (CDS). https://doi.org/10.24381/cds.adbb2d47.

Holman, R.A., Bergsma, E.W.J., 2021. Updates to and performance of the cBathy algorithm for estimating nearshore bathymetry from remote sensing imagery. Rem. Sens. 13, 3996. https://doi.org/10.3390/rs13193996.

Hunt, E., Davidson, M., Steele, E.C.C., Amies, J.D., Scott, T., Russell, P., 2023. Shoreline modelling on timescales of days to decades. Camb. Prisms: Coast. Futures 1 (e16), 1–14. https://doi.org/10.1017/cft.2023.5.

Ibaceta, R., Splinter, K.D., Harley, M.D., Turner, I.L., 2022. Improving multi-decadal coastal shoreline change predictions by including model parameter non-stationarity. Front. Mar. Sci. 9, 1012041. https://doi.org/10.3389/fmars.2022.1012041.

Ibaceta, R., Harley, M.D., Turner, I.L., Splinter, K.D., 2023. Interannual variability in dominant shoreline behaviour at an embayed beach. Geomorphology 433, 108706. https://doi.org/10.1016/j.geomorph.2023.108706.

Kaul, D.T., Vulis, L.M., Schubert, J.E., Sanders, B.F., 2024. Characterizing longshore transport potential and divergence of drift to inform beach loss trends. Coast. Eng. 189, 104473.

Kaminsky, G.M., Ruggiero, P., Gelfenbaum, G.R., 1998. Monitoring coastal change in southwest Washington and northwest Oregon during the 1997/98 El Niño. Shore Beach 66 (3), 42–51.

Kaminsky, G.M., Ruggiero, P., Buijsmain, M., McCandless, D., Gelfenbaum, G., 2010. Historical evolution of the Columbia River littoral cell. Mar. Geol. 273, 96–126. https://doi.org/10.1016/j.margeo.2010.02.006.

Komar, P.D., 1998. El Niño and coastal erosion in the pacific northwest. Shore Beach 60, 57–64.

Komar, P.D., Inman, D.L., 1970. Longshore transport on sand beaches. J. Geophys. Res. 75, 5914–5927.

Komen, G.J., Hasselmann, S., Hasselmann, K., 1984. On the existence of a fully developed wind-sea spectrum. J. Phys. Oceanogr. 14, 1271–1285. https://doi.org/10.1175/1520-0485(1984)014<1271:OTEOAF>2.0.CO;2.

Li, M.Z., Komar, P.D., 1992. Longshore grain sorting and beach placer formation adjacent to the Columbia River. J. Sediment. Petrol. 62, 429–441.

Lowe, R.J., Falter, J.L., Bandet, M.D., Pawlak, G., Atkinson, M.J., Monismith, S.G., Koseff, J.R., 2005. Spectral wave dissipation over a barrier reef. J. Geophys. Res. 110, C04001. https://doi.org/10.1029/2004JC002711.

Lower Columbia Estuary Partnership, 2010. Lower Columbia River digital TerrainModel: lower Columbia estuary partnership website. https://www.estuarypartnership.org/lower-columbia-digital-terrain-model.

Ludka, B.C., Guza, R.T., O'Reilly, W.C., Merrifield, M.A., Flick, R.E., Bak, A.S., et al., 2019. Sixteen years of bathymetry and waves at San Diego beaches. Sci. Data 6, 161. https://doi.org/10.1038/s41597-019-0167-6.

Ludka, B.C., Young, A.P., Guza, R.T., O'Reilly, W.C., Merrifield, M.A., 2023. Alongshore variability of a southern California beach, before and after nourishment. Coast. Eng. 179, 104223. https://doi.org/10.1016/j.coastaleng.2022.104223.

Luijendijk, A., Hagenaars, G., Ranasinghe, R., Baart, F., Donchyts, G., Aarninkhof, S., 2018. The state of the world's beaches. Sci. Rep. 8, 6641. https://doi.org/10.1038/s41598-018-24630-6.

Masselink, G., Castelle, B., Scott, T., Konstantinou, A., 2023. Role of atmospheric indices in describing shoreline variability along the Atlantic coast of Europe. Geophys. Res. Lett. 50, e2023GL106019. https://doi.org/10.1029/2023GL106019.

McCarroll, R.J., Valiente, N.G., Wiggins, M., Scott, T., Masselink, G., 2023. Coastal survey data for perranporth beach and start Bay in southwest england (2006-20021). Sci. Data 10, 258. https://doi.org/10.1038/s41597-023-02131-0.

Moon, J., Song, Y.T., Bromirski, P.D., Miller, A.J., 2013. Multidecadal regional sea level shifts in the Pacific over 1958-2008. J. Geophys. Res.: Oceans 118, 1–12. https://doi.org/10.1002/2013JC009297.

Olabarrieta, M., Warner, J.C., Kumar, N., 2011. Wave-current interaction in Willapa Bay. J. Geophys. Res. 116, C12014.

Palaseanu-Lovejoy, M., Alexandrov, O., Danielson, J., Storlazzi, C., 2023. Satsead: satellite triangulated sea depth open-source bathymetry module for nasa ames stereo pipeline. Rem. Sens. 15 (16), 3950.

Pearson, S.G., van Prooijen, B.C., Elias, E.P.L., Vitousek, S., Wang, Z.B., 2020. Sediment connectivity: a framework for analyzing sediment transport pathways. J. Geophys. Res.: Earth Surf. 125, e2020JF005595. https://doi.org/10.1029/2020JF005595.

Peterson, C.D., Jackson, P.L., O'Neil, D.J., Rosenfeld, C.L., Kimerling, A.J., 1990. Littoral cell response to interannual climatic forcing 1983-1987 on the central Oregon coast, USA. J. Coast Res. 6 (1), 87–110.

Ranasinghe, R., McLoughlin, R., Short, A., Symonds, G., 2004. The Southern Oscillation Index, wave climate, and beach rotation. Mar. Geol. 204, 273–287.

Rasmussen, R.M., Chen, F., Liu, C.H., Ikeda, K., Prein, A., Kim, J., et al., 2023. CONUS404: the NCAR–USGS 4-km long-term regional hydroclimate reanalysis over the CONUS. Bull. Am. Meteorol. Soc. 104 (8), E1382–E1408. https://doi.org/10.1175/BAMS-D-21-0326.1.

Ritchie, A.C., Warrick, J.A., East, A.E., Magirl, C.S., Stevens, A.W., Bountry, J.A., et al., 2018. Morphodynamic evolution following sediment release from the world's largest dam removal. Sci. Rep. 8, 13279. https://doi.org/10.1038/s41598-018-30817-8.

Roegner, G.C., Fields, S.A., Henkel, S.K., 2021. Benthic video landers reveal impacts of dredged sediment deposition events on mobile epifauna are acute but transitory. J. Exp. Mar. Biol. Ecol. 538, 151526. https://doi.org/10.1016/j.jembe.2021.151526.

Ruggiero, P.R., Kaminsky, G.M., Gelfenbaum, G., Voigt, B., 2005. Seasonal to interannual morphodynamics along a high-energy dissipative littoral cell. J. Coast Res. 21, 553–578.

Ruggiero, P., Komar, P.D., Allan, J.C., 2010a. Increasing wave heights and extreme value projections: the wave climate of the U.S. Pacific Northwest. Coast. Eng. 57, 539–552. https://doi.org/10.1016/j.coastaleng.2009.12.005.

Ruggiero, P., Buijsman, M.C., Kaminsky, G., Gelfenbaum, G., 2010b. Modeling the effect of wave climate and sediment supply variability on large-scale shoreline change. Mar. Geol. 273, 127–140. https://doi.org/10.1016/j.margeo.2010.02.008.

Ruggiero, P., Kratzmann, M.G., Himmelstoss, E.A., Reid, D., Allan, J., Kaminsky, G.M., 2013. National assessment of shoreline change—historical shoreline change along the Pacific Northwest coast. U.S. Geol. Surv. Open-File Rep. 2012–1007, 62. https://doi.org/10.3133/ofr20121007.

Ruggiero, P., Kaminsky, G.M., Gelfenbaum, G., Cohn, N., 2016. Morphodynamics of prograding beaches—a synthesis of seasonal- to century-scale observations of the Columbia River littoral cell. Mar. Geol. 376, 51–68.

Saunders, T.M., Cohn, N., Hesser, T., 2024. Insights into nearshore sandbar dynamics through process-based numerical and logistic regression modeling. Coast. Eng. 104558.

Shepard, F.P., 1950. Beach Cycles in Southern California. U.S. Army Corps of Engineers, Washington D.C., p. 26. Technical Report Memorandum 20.

Splinter, K.D., Gonzalez, M.V.G., Oltman-Shay, J., Rutten, J., Holman, R., 2018. Observations and modelling of shoreline and multiple sandbar behaviour on a high-energy meso-tidal beach. Continent. Shelf Res. 159, 33–55.

Splinter, K.D., Coco, G., 2021. Challenges and Opportunities in coastal shoreline protection. Front. Mar. Sci. 8, 788657. https://doi.org/10.3389/fmars.2021.788657.

Stevens, A.W., Gelfenbaum, G., Ruggiero, P., Kaminsky, G.M., 2012. Southwest Washington littoral drift restoration—beach and nearshore morphological monitoring. U.S. Geol. Surv. Open-File Rep. 2012–1175, 67.

Stevens, A.W., Weiner, H.M., Wood, J.M., Ruggiero, P., Kaminsky, G.M., Gelfenbaum, G. R., 2019. Beach topography and nearshore bathymetry of the Columbia River littoral cell, Washington and Oregon (ver. 4.0, January 2024). U.S. Geol. Surv. Data Release. https://doi.org/10.5066/P9W15JX8.

Stevens, A.W., Elias, E., Pearson, S., Kaminsky, G.M., Ruggiero, P.R., Weiner, H.M., Gelfenbaum, G.R., 2020. Observations of coastal change and numerical modeling of sediment-transport pathways at the mouth of the Columbia River and its adjacent littoral cell. U.S. Geol. Surv. 82. https://doi.org/10.3133/ofr20201045. Open-File Report 2020–1045.

Stevens, A.W., Moritz, H.R., Elias, E.P.L., Gelfenbaum, G.R., Ruggiero, P.R., Pearson, S. G., et al., 2023. Monitoring and modeling dispersal of a submerged nearshore berm at the mouth of the Columbia River, USA. Coast. Eng. 181, 104285.

Stevens, A.W., Parker, K.A., Vitousek, S., 2024. Modeled nearshore wave parameters along the Columbia River littoral cell, Washington and Oregon, 2010-2023. U.S. Geol. Surv. Data Release. https://doi.org/10.5066/P1R9REKP.

Szafarczyk, A., Tos, C., 2022. The use of green laser in LiDAR bathymetry, state of the art and recent advancements. Sensors 23, 292. https://doi.org/10.3390/s23010292.

Turner, I.L., Harley, M.D., Short, A.D., Simmons, J.A., Bracs, M.A., Phillips, M.S., Splinter, K.D., 2016. A multi-decade dataset of monthly beach profile surveys and inshore wave forcing at Narrabeen, Australia. Sci. Data 3, 160024. https://doi.org/10.1038/sdata.2016.24.

Twichell, D.C., Cross, V.A., Peterson, C.D., 2010. Partitioning of sediment on the shelf offshore of the Columbia River littoral cell. Mar. Geol. 273, 11–31. https://doi.org/10.1016/j.margeo.2010.02.001.

USACE, 2023. Annual Use Plan. Management of Open Water Dredged Material Placement/Disposal Sites; Mouth of the Columbia River, OR and WA. U.S. Army Corps of Engineers Portland District, p. 107. https://www.nwp.usace.army.mil/Portals/24/docs/navigation/LCRCMP/MCR_AUP_2023.pdf. (Accessed 30 April 2024).

Vitousek, S., Barnard, P.L., Limber, P., Erikson, L., Cole, B., 2017. A model integrating longshore and cross-shore processes for predicting long-term shoreline response to climate change. J. Geophys. Res.: Earth Surf. 122, 782–806. https://doi.org/10.1002/2016JF004065.

Vitousek, S., Buscombe, D., Vos, K., Barnard, P.L., Ritchie, A., Warrick, J.A., 2022. The future of coastal monitoring through satellite remote sensing. Camb. Prisms: Coast. Futures 1 (e10), 1–18. https://doi.org/10.1017/cft.2022.4.

Vitousek, S., Vos, K., Splinter, K.D., Erikson, L., Barnard, P.L., 2023. A model integrating satellite-derived shoreline observations for predicting fine-scale shoreline response to waves and sea-level rise across large coastal regions. J. Geophys. Res. Earth Surf. 128, e2022JF006936. https://doi.org/10.1029/2022JF006936.

Vos, K., Harley, M.D., Turner, I.L., Splinter, K.D., 2023. Pacific shoreline erosion and accretion patterns controlled by El Niño/Southern Oscillation. Nat. Geosci. 16, 140–146. https://doi.org/10.1038/s41561-022-01117-8.

Warrick, J.A., Vos, K., East, A.E., Vitousek, S., 2022. Fire (plus) flood (equals) beach: coastal response to an exceptional river discharge event. Sci. Rep. 12, 3848. https://doi.org/10.1038/s41598-022-07209-0.

Wiberg, P.L., Sherwood, C.R., 2008. Calculating wave-generated bottom orbital velocities from surface-wave parameters. Comput. Geosci. 34, 1243–1262. https://doi.org/10.1016/j.cageo.2008.02.010.

Wiggins, M., Scott, T., Masselink, G., Russell, P., McCarroll, R.J., 2019. Coastal embayment rotation: response to extreme events and climate control, using full embayment surveys. Geomorphology 327, 385–403.

Willmott, C.J., 1982. Some comments on the evaluation of model performance. Bull. Am. Meteorol. Soc. 63, 1309–1313.

Wright, L.D., Short, A.D., 1984. Morphodynamic variability of surf zones and beaches: a synthesis. Mar. Geol. 56, 93–118.